



DOI: 10.18720/MCE.94.9

Two-way patched RC slabs under concentrated loads

S.A. Kristiawan*, A. Supriyadi

^a Universitas Sebelas Maret, Surakarta, Indonesia,

* E-mail: s.a.kristiawan@ft.uns.ac.id

Keywords: patching, slab, spalling, ultimate load, unsaturated polyester resin mortar, yield line

Abstract. Damage that occurs in reinforced concrete elements can reduce the capacity and serviceability of these elements. One of the damages that may be encountered is spalling or delamination of concrete covers. Repairs to this type of damage can be carried out by patching methods. This research uses unsaturated polyester resin mortar (UPR-mortar) as a patch repair material to recover the damage of two-way slabs. Laboratory investigations were carried out to determine the effects of variations in patching location and loading on the ultimate capacity. The development of crack patterns as the load increases, the final yield lines formed at the time of collapse, and the magnitude of the ultimate load are the main data discussed in this research. In addition, load-deflection behavior, stiffness and toughness are also presented and discussed. Yield Line Theory (YLT) has been applied using virtual work principle with several assumptions and simplifications to estimate the ultimate load of the slabs. The experimental results show that UPR-mortar is able to recover the capacity and stiffness of the damaged slab, but it can not restore the toughness to the original level. The theoretical strength of the patched repair slabs estimated by simplified YLT shows that it is at least 90 % compared to experimental results.

1. Introduction

Reinforced concrete slab is widely used as floor elements in multi-story building structures. One type of slabs that is commonly found is rectangular slab which is supported on all four sides. This type of slab is known as a two-way slab. As part of structural system, reinforced concrete slab must be designed in such a way that they have sufficient capacity to be able to bear all the load combinations that the building will receive. The adequacy of the slab capacity in carrying the load can be expressed from the value of the safety factor. The structural concrete designers refer to Codes of Practice to ensure that the value of this safety factor is met [1, 2]. In reality, we must realize that the ultimate strength of slab may decrease along with the life of the building, and so it lowers the safety factor level over time. There are several factors that can reduce the value of this strength, for example, the degradation of concrete components that arise a result of high intensity of seismic load [3], fire exposure [4], reinforcement corrosion [5, 6], etc. In the case of reinforcement corrosion, the degradation of concrete components can be in the form of cracking, spalling and delamination of concrete covers [7–11]. In such situation, it is necessary to repair the damaged concrete components and corroded reinforcement so that the strength and serviceability of reinforced concrete slabs are restored. Several methods can be used to repair such damage including patching [12–14] and strengthening [15–24] with various materials and techniques. In term of patching, this method requires patch repair material which must meet several criteria including compatibility in mechanical properties, compatibility in dimensional properties, and compatibility in durability [13, 25–30]. One potential repair material that meets these criteria is unsaturated polyester resin mortar or UPR-mortar [31–34].

The ability of UPR-mortar in recovering the capacity of reinforced concrete slab patched with this material can be demonstrated by comparing the ultimate capacity of the patched repair RC slab with the normal RC slab. The ultimate capacity of reinforced concrete slab can be determined from the loading test results and estimated through theoretical calculations. In the loading test, ultimate capacity refers to when the slab is no longer able to bear an increase in load before it finally collapses [17, 34–37]. When the slab reaches the collapse phase, the crack lines show a certain pattern that can explain the mechanism of slab collapse. Crack lines that describe the collapse mechanism are also known as yield lines. Yield line pattern is an important parameter that is interesting to study because it becomes the basis in estimating the ultimate load of reinforced concrete slabs according to Yield Line Theory or YLT [38–42].

Kristiawan, S.A., Supriyadi, A. Two-way patched RC slabs under concentrated loads. Magazine of Civil Engineering. 2020. 94(2). Pp. 108–119. DOI: 10.18720/MCE.94.9



This work is licensed under a CC BY-NC 4.0

In principle, YLT assumes that reinforced concrete slabs have a uniform cross section and has a flexural collapse mode. Other important variables that influence the analysis according to this theory include the type of boundary conditions and the pattern of loading. In the case of reinforced concrete slabs that have been patched with UPR-mortar, the existence of patching zones makes the uniformity assumption unfulfilled. In the case of patched repair one-way slabs that carry a concentrated load in the center of the slabs, it has been shown that patching zones cause changes in yield line patterns and consequently ultimate load values also change [34].

Calculation of ultimate load according to YLT can be explained briefly as follows [43]. When the slab collapse mechanism occurs, the yield line is seen as the axis of rotation of the slab segments. The slab support line also acts as a rotation axis. The ultimate moment capacity (m_u) of reinforced concrete slabs per 1 m wide for a given reinforcement ratio can be calculated by Equation (1) as follows:

$$m_u = A_s \cdot f_y \cdot \left(d - 0.59 \cdot A_s \cdot \frac{f_y}{f_c} \right), \quad (1)$$

where A_s is the area of tensile reinforcement per meter width of the slab, f_y the yield stress of the steel reinforcement, f_c concrete compressive strength, d the distance between the center of the tensile reinforcement and the outer concrete compressive fiber. In certain cases, it is often necessary to determine the ultimate bending moment capacity along the yield line that has a direction not the same as the main axis of reinforcement of the slab. If the ultimate bending moments per unit width in the x and y directions respectively are m_{ux} dan m_{uy} , then the ultimate bending moment in any yield line (m_{un}) is obtained from Johansen's criteria (Figure 1), and is expressed in Equation (2) as follows:

$$m_{un} = m_{ux} \cos^2 \alpha + m_{uy} \sin^2 \alpha, \quad (2)$$

where the x and y axes are the reinforcement slabs, while α is the angle formed by the direction of the yield line with the y axis (see Figure 1).

The yield line pattern obtained from experimental investigations was used as validity for the assumption of location and yield line orientation that occurred on reinforced concrete slabs. Ultimate load P_u calculation was derived by the virtual work method [41]. Internal work done by the bending moment that occurs on the slab is $\sum m_{un} \cdot \theta_n \cdot L_o$ where θ_n is the relative rotation angle of the two slab segments to a yield line (Figure 2) and L_o is the length of the yield line. External work done by external forces in the form of concentrated load is $\sum P_u \cdot \Delta$, where P_u is the ultimate load, and Δ is slab deflection. The principle of virtual work states that external work is equal to internal work as expressed in Equation (3):

$$\sum m_{un} \cdot \theta_n \cdot L_o = \sum P_u \cdot \Delta. \quad (3)$$

The value of θ_n is explained by Figure 2 which is $\Delta / b_1 + \Delta / b_2$.

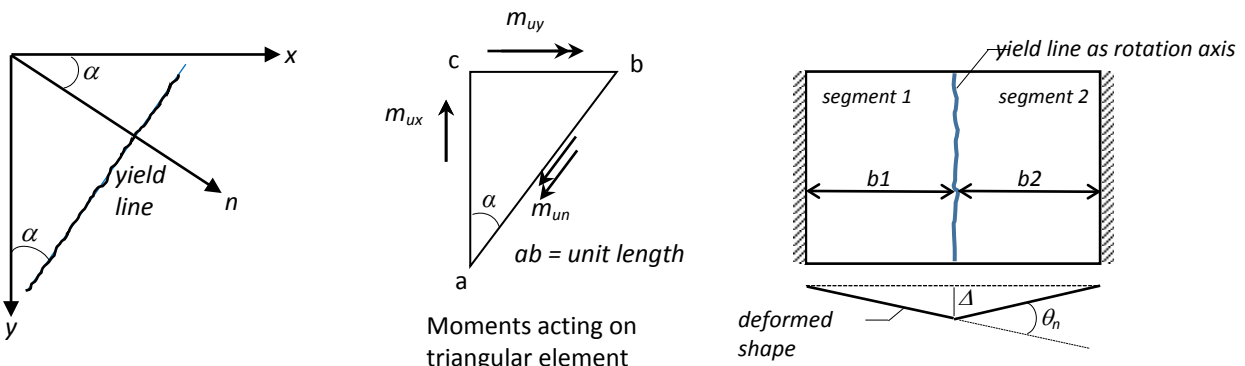


Figure 1. Yield line at general angle to orthogonal slab reinforcement.

Figure 2. Rotation of slab segments (θ_n) about each yield line.

Previous study suggests that UPR-mortar could be used to repair a damage on one-way slabs under concentrated load applied at the center of the slabs. Both experimental results and theoretical calculation using simplified YLT confirm the capability of UPR-mortar to restore the strength of the damaged slabs [34]. The results of the previous study encourage researchers to further investigate the application of UPR-mortar to restore more general cases of spalled reinforced concrete slabs. This research aims to determine the influence of patching zone locations on their associated yield line patterns and ultimate loads for the two-way

slab type. In addition to the patching zone variable, this research will also include an investigation on the effect of location/position of a concentrated load. Both experimental investigation and theoretical calculation of ultimate load using simplified YLT will be covered in this research.

2. Methods

In this research, 8 (eight) reinforced concrete slab specimens have been made with size (length×width×thickness) each of which is 1350×950×80 mm. In the short direction, the steel reinforcements are 7D10mm, while in the long direction they are 5D10mm (Figure 3). The first slab represents normal reinforced concrete slab without damage. The second slab represents reinforced concrete slab with spalling dimensions 300×200×30 mm and no patching. The spalling is simulated by cut out. The other six slabs represent spalling of reinforced concrete slabs but they have been patched with UPR-mortar with variations in patching locations. The types of slab specimens, identity, and parameter variations are summarized in Table 1 and 3.

Table 1. Types of reinforced concrete slab specimens.

Slab identity	Slab type, patching position, and concentrated load (P) position
N	Normal slab, without spalling (cut out), centric load
R0	Unrepaired slab, with spalling (cut out) but no patching, centric load
R1	Repaired slab, centric patching, centric load
R2	Repaired slab, eccentric patching, centric load
R3	Repaired slab, eccentric patching, centric load
R4	Repaired slab, eccentric patching, centric load
R5	Repaired slab, eccentric patching, eccentric load
R6	Repaired slab, eccentric patching, eccentric load

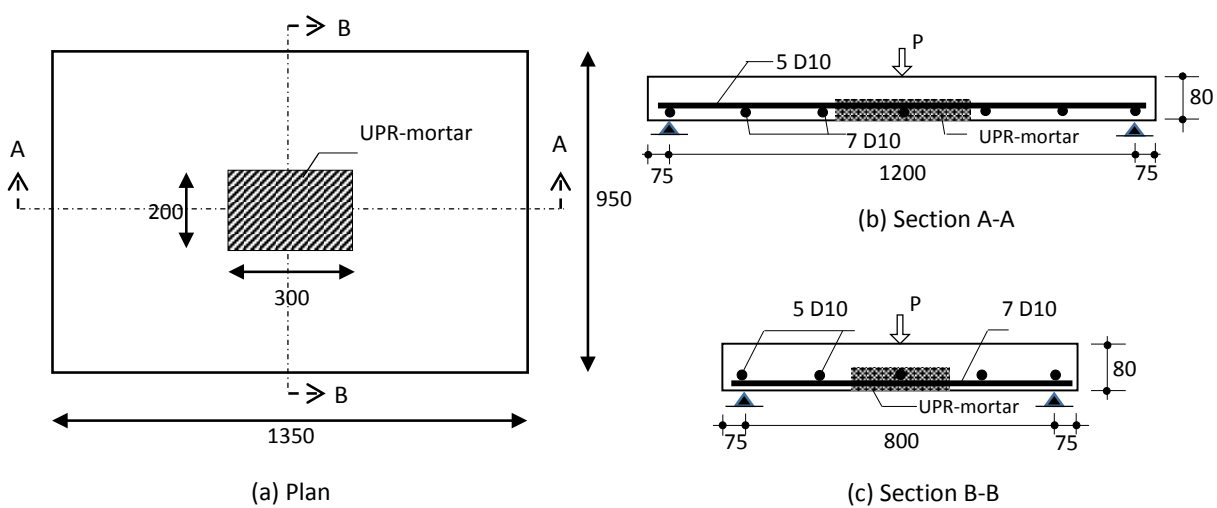


Figure 3. Slab size, reinforcement, patching position and load on plate specimen R1.

The slab size, reinforcement, patching position and load of one of specimen of reinforced concrete slabs (R1) are shown in Figure 3. The average compressive strength of concrete used to make reinforced concrete slabs was 29.47 MPa, while the tensile strength of reinforcing steel was 350.52 MPa. After the reinforced concrete slab has been casted, the curing process was done by wetting the specimen with water for 21 days and continued by storing the specimen in a laboratory environment for 3 months. After 3 months in a laboratory environment, reinforced concrete slabs were prepared for a load test. One day before the load test was carried out, the slabs (except slab N and R0) were patched first with a UPR mortar. UPR mortar was made with materials and composition: 950 kg of sand, 808 kg of cement, 143 kg of fly ash, 475 kg of UPR, and 14.25 kg of hardener per m³. This UPR mortar composition gave an average compressive strength of 75 MPa and a tensile strength (flexural) of 24.6 MPa when tested at 1 day of age.

All specimens of reinforced concrete slabs were laid on four sides with a simple-support type. The distance between the supports in the short and long spans were 800 mm and 1200 mm, respectively (Figure 3). External force in the form of concentrated load were applied according to their variations (Table 3). The load was applied to the slab at an increment of 0.5 kN. The maximum deflection that occurred under load was measured by a dial gauge. Observation of the crack pattern that occurred at the bottom of the slab was done from the initial load until the slab collapses. Figure 4 illustrates an example of testing on one of the slabs.

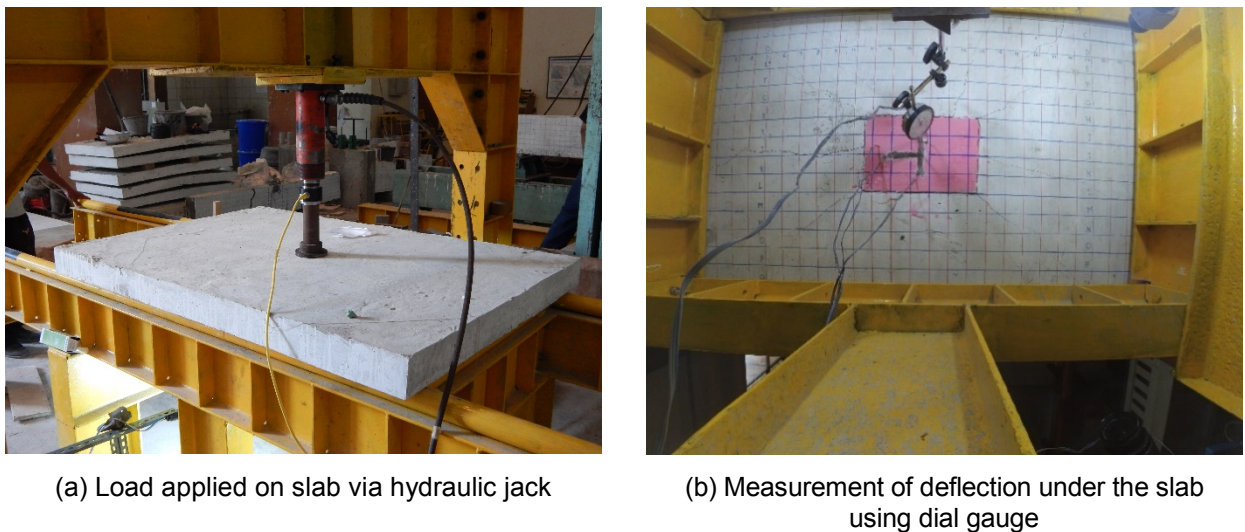


Figure 4. Overview of loading and measurement of deflection on the slab.

3. Results and Discussion

3.1. Effects of Patching on the Development of Crack Pattern

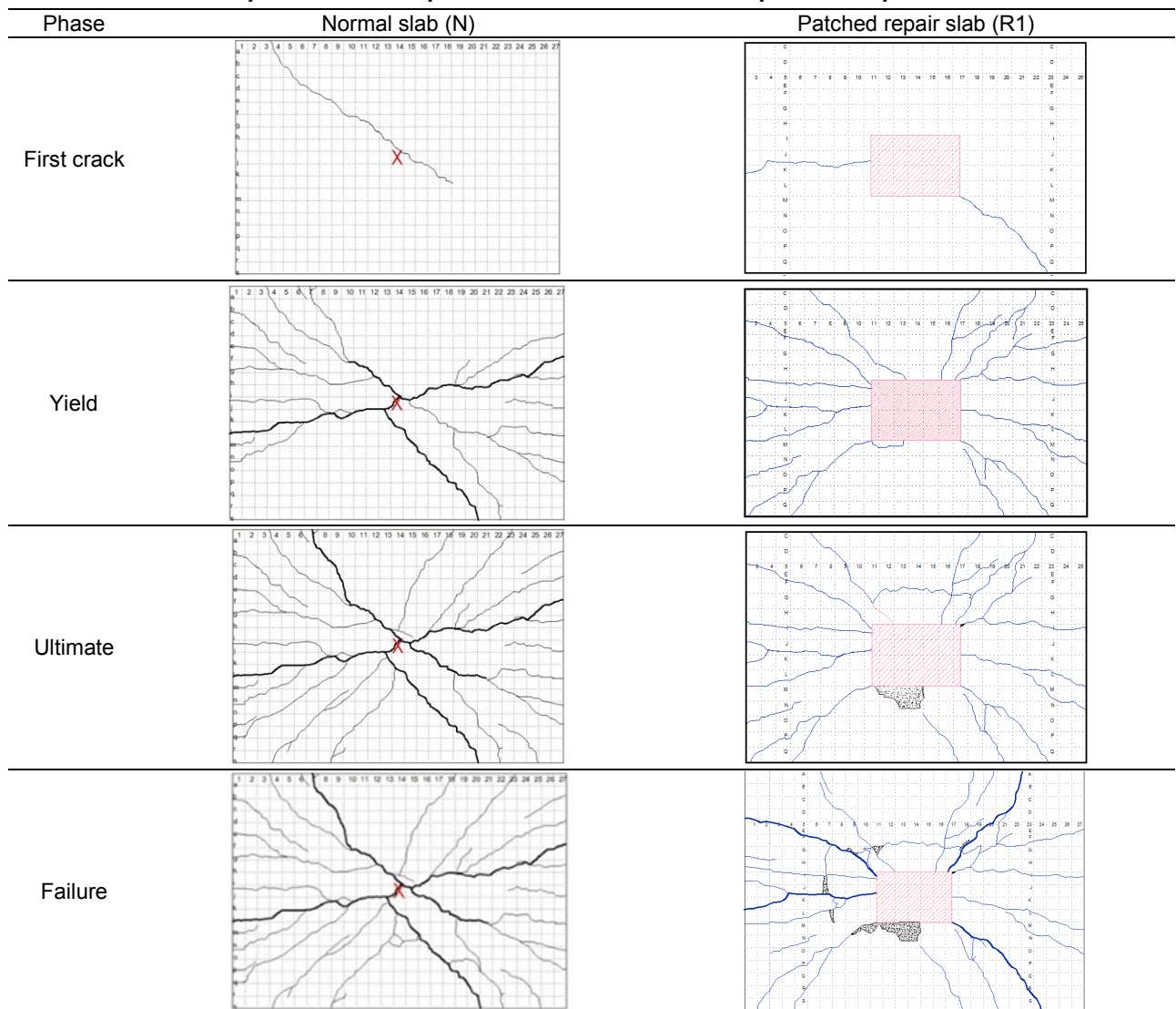
Table 2 shows the development of crack patterns as load increases. At the initial phase before the first crack occurs, the distribution of the bending moment at the cross section of the slab follows the elastic theory. After a crack occurs, it causes a decrease in the stiffness of slab at the cracked section; consequently, it leads to a change in the moment distribution. At the tensile zone of the cracked section, a higher tensile stress is transferred to the steel reinforcements. Further increase of load causes the steel reinforcements at this cracked section reach their yielding stress. This crack forms the first yield line. Increasing load after the first yield line will produce more cracks to form a number of yield lines which divided the plane of the slab into several segments that incite the collapse mechanism. When the collapse mechanism has been formed, the slab reaches a phase of failure [38, 40].

Table 2 also illustrates the comparison of the development of crack patterns that occur on one of the slabs that have been repaired with UPR-mortar (slab R1) compared to normal slab (slab N), starting from the first crack, yield, ultimate and failure phases. In the first crack phase, it is shown that patching causes the crack to occur not starting in the middle of the slab, but outside the patched area. Meanwhile, for normal slab, cracks are initiated from the center of the slab where maximum moments occurred. In subsequent phases (yield, ultimate, and failure), it is also shown that the crack line never crossed the patched area. In terms of crack intensities that occurred in slab N and slab R1, they show similarities. This indicates that patching with UPR-mortar produces slab which have the ability to redistribute bending moments well before collapse, as in the case of normal slab [34].

3.2. Effect of Patching and Load Position on Final Crack Pattern

The influence of patching area and concentrated load positions to the crack patterns are also examined in this research. Variations in the positions of the patching area include: centric position in the middle of the slab plane, eccentric on one axis, and eccentric on two axes. Variations of concentrated load positions are similar to patching area. The influence of patching area and load positions to the final crack patterns that describe the collapse mechanism of each slab and their corresponding ultimate load are presented in Table 3.

Generally, due to concentrated load, crack patterns in the collapse phase tend to form curves with radial lines forming circular fan patterns [34, 35]. This is different from the crack pattern in the slab with evenly distributed loads, which form triangular patterned segments between the yield lines [43]. Concentrated load position has a significant effect on crack patterns. The area under the concentrated load is a potential position for the initial crack. The development and propagation of the crack lines in the radial direction is started from the point under this concentrated load. When the concentrated load is placed at the center of the slabs or centric to the slab axes (N, R0, R1, R2 and R3), the crack lines is started in this point as well with the exception of R1. The present of patching on the center of the slab causes the crack lines occur outside the patching area. This is because the patching material (UPR-mortar) possess a higher tensile stress (about 24.6 MPa) compared to substrate concrete (about 3-7 MPa). Hence, the maximum bending moment at the center of the R1 does not initiate crack in this area. Meanwhile, when the concentrated load is shifted to be an eccentric to the axes (R4, R5, R6), it is seen that the starting point of the crack lines is also shifted following the load position. In all cases, the crack lines never cross the patched zone. This finding confirms the previous results [34].

Table 2. Development of crack patterns on normal slab and patched repair slab.

loading position

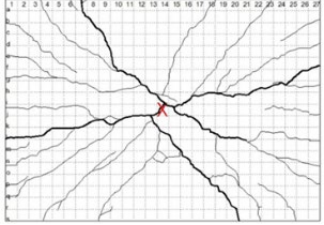
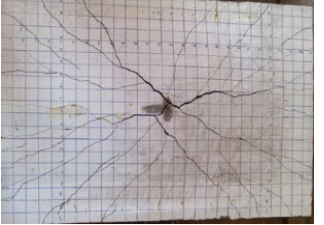
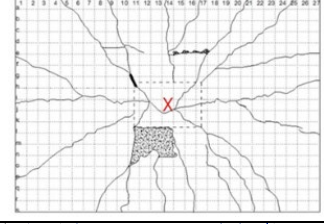
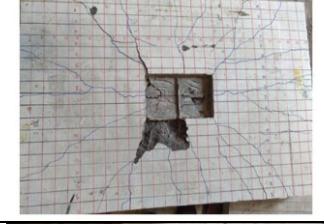
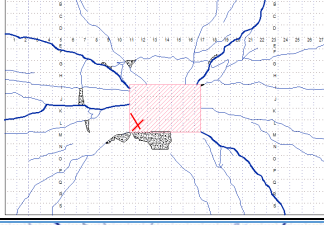
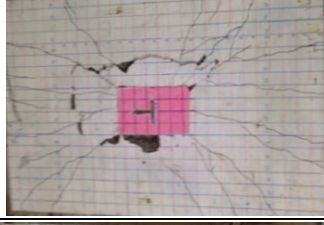
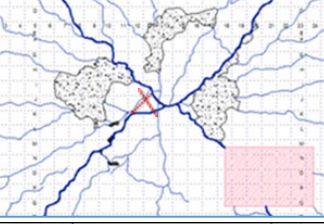
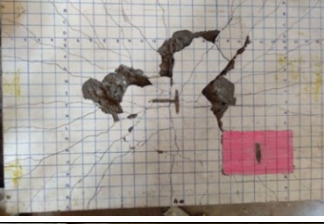
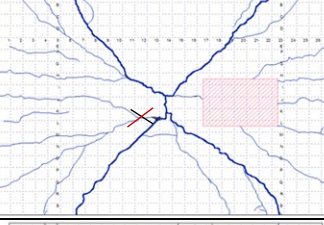
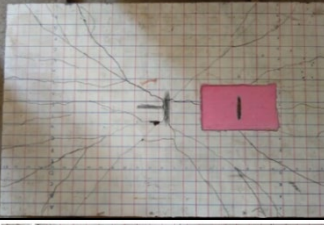
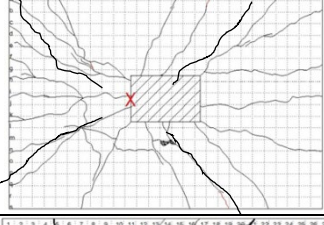
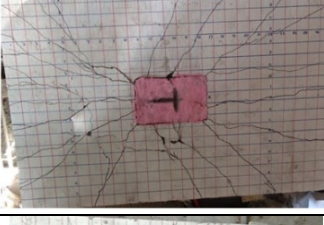
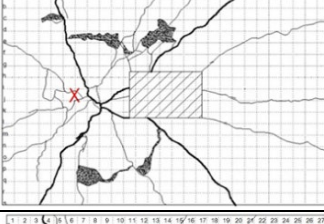
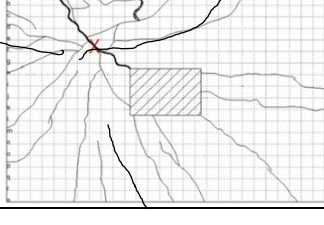
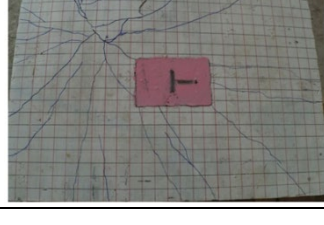
Table 3 also indicates the failure mode observed on slabs during the experimental investigation. Not all slabs exhibit flexural mode failure, but some slab specimens show punching shear mode failure (slabs R0, R1 and R5). This punching shear is marked by the sinking of the steel plate which is used to transfer the concentrated load to the slab (Figure 5. (b)). Additional failure mode in the form of delamination is also noticed in slab R1 (Figure 5 (a)). Since this delamination is only occur in R1, it is of interest to investigate more detail on the bond between patching material and concrete substrate in this slab. It was noticed that when the patching material was applied to fill the cut out of the slab R1, the patching material did not entirely seal the cut out. There was a gap between the interface of cut out and patching material at one of the perimeters. This gap eventually triggered a “push off” when concentrated load was applied.

It is also interesting to note the effect of the supports. The slabs were laid on four supports without any restraints against upward displacement. Hence, when the concentrated load was imposed, it caused uplift at the corner of the supports. This uplift of the corner slab caused the yield lines direction to shift i.e. the yield lines did not form toward the corner point of the slabs as theoretically expected [38], instead they were diverted toward the side of the slabs. With this kind of yield line patterns, the slab's ultimate load will be lower than the pattern with yield lines toward the corner.

3.3. Ultimate load

The results of experimental investigations demonstrate how spalling on reinforced concrete slab (represented by cut out of slab R0) significantly causes a reduction in slab ultimate strength. From Table 3, it can be shown that the ultimate load (P_u) of R0 is 50.35 kN or 75.5 % to that of normal slab (N). The cut out reduces the thickness of the slab; consequently this thickness reduction leads to decrease in both the bending moment capacity [44] and punching shear capacity [45]. In the case of slab R0, reduction of punching shear capacity is more critical as shown by the emerged punching failure mode of this particular slab. Comparing the ultimate load of R0 and R1, R2, and R3, it is also confirmed that patching with UPR-mortar could restore the ultimate strength of the slabs to a level close to the original strength (N) with the exception of R1. The lower ultimate load of the R1 could be related to the failure mode of this slab as explained in the previous section.

Table 3. Final crack pattern of slabs and their ultimate load.

Type of slab	Sketch of final crack pattern	Bottom surface of slab after failure	Ultimate load and failure mode
Slab N			$P_{u,ex} = 66.68 \text{ kN}$ Flexural failure
Slab R0			$P_{u,ex} = 50.35 \text{ kN}$ Punching shear
Slab R1			$P_{u,ex} = 53.07 \text{ kN}$ Punching shear and delamination of patching material
Slab R2			$P_{u,ex} = 69.40 \text{ kN}$ Flexural failure
Slab R3			$P_{u,ex} = 63.05 \text{ kN}$ Flexural failure
Slab R4			$P_{u,ex} = 50.80 \text{ kN}$ Flexural failure
Slab R5			$P_{u,ex} = 57.61 \text{ kN}$ Punching shear
Slab R6			$P_{u,ex} = 60.78 \text{ kN}$ Flexural failure

 loading position

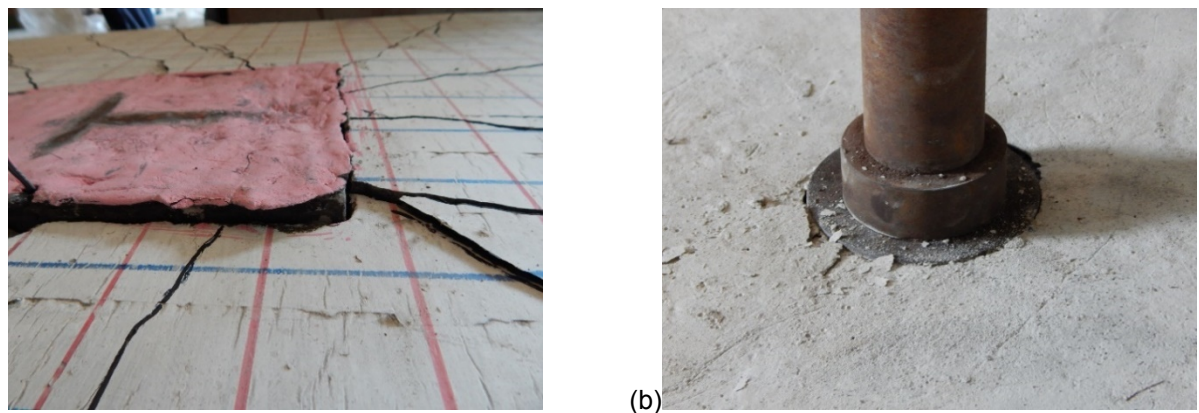
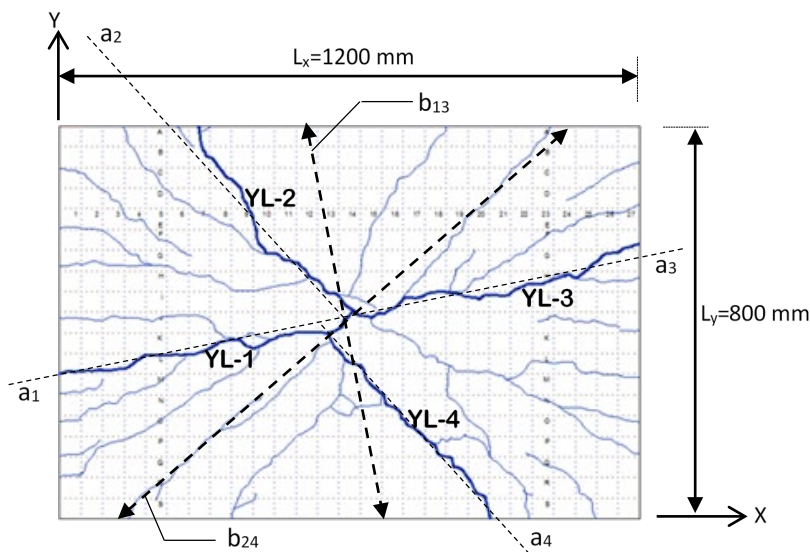


Figure 5. (a) Delamination of patching material UPR-mortar; (b) Punching shear in slabs.

The ultimate load of R4, R5, R6 represent the ultimate load of slab where the concentrated load is applied eccentric. It is unfortunate that we did not test a normal slab with an eccentric applied load to confirm the capability of the UPR-mortar in restoring the strength of the damaged slab. However, comparison of theoretical and experimental ultimate load can be used to indicate the strength recovery after patching with UPR-mortar as discussed in the following paragraphs.

Ultimate load of the slabs has been obtained from experimental investigations ($P_{u, ex}$). In this section, the value of $P_{u, ex}$ will be compared with a theoretical approach based on yield line theory (YLT). In using this theory, it is assumed that the cross section of the slab per unit width is the same. It is supposed that the presence of UPR-mortar will cause this assumption to be incorrect. However, in the context of simplification of ultimate load calculation, the assumption of uniformity is maintained. The influence of the patching is only taken into account in relation to the changes in the yield line patterns that occur between normal and patched slab. The yield line pattern will affect the estimated ultimate load as described in the next section. Thus, simplification in this theoretical approach was merely derived from the pattern of yield lines. Meanwhile, the various types of collapse (flexure, punching, delamination) and the phenomenon of corner levers are also ignored.



Notation:

YL-1, YL-2, YL-3, YL-4 = yield lines

a_1, a_2, a_3, a_4 = yield line slope direction (YL-1, YL-2, YL-3, YL-4)

b_{13} = length component to calculate the rotation angle θ_n on YL-1 and YL-3

b_{24} = length component to calculate the rotation angle θ_n on YL-2 and YL-4

Figure 6. Calculation of P_u on a normal plate with the virtual work method.

Figure 6 shows the yield line pattern on the normal slab (N) used to calculate P_u by the virtual work method. The calculated data used are as follows. Slab span in the long and short direction respectively are 1200 mm and 800 mm. The tensile strength of steel reinforcement is 350.5 MPa and the compressive strength of concrete is 29.47 MPa. Flexural reinforcements in the long direction are 5D10 mm ($A_s = 392.7 \text{ mm}^2$), while in the short direction are 7D10 mm ($A_s = 549.78 \text{ mm}^2$). With a slab thickness of 80 mm, the effective heights (d) in the long and short direction are 45 mm and 55 mm, respectively. By using Equation (1), the ultimate bending

moment capacity per 1 m width of the slab in the long direction (m_{ux}) and in the short direction (m_{uy}) are respectively 6,535,305 N.mm and 7,705,521 N.mm. The yield line of YL-1, YL-2, YL-3 and YL-4 are formed at an angle α to the y-axis successively at 80°, 42°, 80°, and 42°. By using Equation (2), an ultimate bending moment is obtained for each yield line (m_{un}) respectively of 7,670,235 N.mm, 7,059,252 N.mm, 7,670,235 N.mm and 7,059,252 N.mm. The length of each yield line (L_o) is respectively 0.609 m, 0.538 m, 0.609 m, and 0.538 m. With the length components of $b1$ and $b2$ for YL-1 (see Fig. 1), each is 406.2 mm and Δ (deflection of slab under loading) measured from experiments of 30.89 mm, a rotation angle (θ_n) is obtained for 0.1521 radians. In the same way, values (θ_n) for YL-2, YL-3 and YL-4 are respectively 0.1033 radians, 0.1521 radians and 0.1033 radians. Internal work (W_i) is calculated from the left-hand section of Equation (3) of 2,206,971 N.mm. Finally, with Equation (3), the ultimate load value (P_u) for normal slab is 71,446 N or 71,446 kN. The ratio of theoretical P_u values to experimental P_u ($R = P_u/P_{u, ex}$) is 1.07.

In the same way, the P_u is calculated for each slab according to its corresponding crack pattern and the results are presented in Table 4. The results of calculation by simplified YLT theory show that the ultimate strength is at least 90 % compared to the experimental result, except for slab R2. The possible reason of lower value of theoretical ultimate load of R2 compared to that of the experimental value could be traced from the crack's intensity. As shown in Table 3, the slab shows a greater intensity of cracks before failure. This intensity of cracks indicates that the R2 slab capable to redistribute the bending moment at high load level. Hence, the obtained experimental ultimate load is appreciately high (69.4 kN). Meanwhile, the simplified YLT does not consider the intensity of cracks for estimating the ultimate load.

Table 4. The estimated results of the ultimate load value (P_u) based on YLT.

Slab	YL	α (°)	m_{un} (N.mm)	L_o (m)	Δ (mm)	$b1$ (mm)	$b2$ (mm)	θ_n (rad)	W_i (N.mm)	P_u (kN)	$P_{u, ex}$ (kN)	R
N	YL-1	80	7,670,235	0.609	30.89	406.2	406.2	0.1521	2,206,971	71.446	66.68	1.07
	YL-2	42	7,059,252	0.538		597.8	597.8	0.1033				
	YL-3	80	7,670,235	0.609		406.2	406.2	0.1521				
	YL-4	42	7,059,252	0.538		597.8	597.8	0.1033				
R1	YL-1	80	7,670,235	0.457	9.15	507.7	304.6	0.0481	522,181	57.069	53.07	1.08
	YL-2	70	7,568,632	0.479		532.1	319.3	0.0459				
	YL-3	40	7,018,810	0.392		466.7	777.9	0.0314				
	YL-4	35	6,920,294	0.523		523.0	871.7	0.0280				
R2	YL-1	43	7,079,598	0.547	18.12	546.9	586.5	0.0640	982,937	54.246	69.4	0.78
	YL-2	45	7,120,413	0.566		565.7	565.7	0.0641				
	YL-3	42	7,059,252	0.538		538.3	597.8	0.0640				
	YL-4	40	7,018,810	0.522		522.2	522.3	0.0638				
R3	YL-1	45	7,120,413	0.566	18.06	565.7	565.7	0.0639	1,028,757	56.963	63.05	0.90
	YL-2	45	7,120,413	0.566		565.7	565.7	0.0639				
	YL-3	45	7,120,413	0.566		565.7	565.7	0.0639				
	YL-4	45	7,120,413	0.566		565.7	565.7	0.0639				
R4	YL-1	40	7,018,810	0.522	14.27	622.3	622.3	0.0459	707,474	49.578	50.80	0.98
	YL-2	40	7,018,810	0.522		622.3	622.3	0.0459				
	YL-3	45	7,120,413	0.566		565.7	565.7	0.0505				
	YL-4	40	7,018,810	0.522		622.3	622.3	0.0459				
R5	YL-1	25	6,744,312	0.386	10.69	331.0	828.2	0.0452	566,929	53.034	57.61	0.92
	YL-2	25	6,744,312	0.497		331.0	1064.8	0.0423				
	YL-3	40	7,018,810	0.587		700.1	456.9	0.0387				
	YL-4	45	7,120,413	0.495		424.3	636.4	0.0420				
R6	YL-1	40	7,018,810	0.392	6.53	587.4	466.7	0.0251	383,376	58.710	60.78	0.97
	YL-2	70	7,568,632	0.585		212.8	638.5	0.0409				
	YL-3	30	6,827,859	0.346		600.0	1,000.0	0.0174				
	YL-4	70	7,568,632	0.319		212.8	877.1	0.0381				

3.4. Load-Deflection Behavior

Global response of slabs under concentrated load could be characterised by the load-deflection behaviour. Figure 7 shows the load-deflection behaviours of the investigated slabs, which are presented into three groups. The first group (Figure 7 (a)) are slabs with centric imposed of concentrated load (N, R0, R1) but each slab represents respectively normal, cut out without being repaired, and patch repaired slab. This group (Figure 7 (b)) is intended to show the influence of spalling (cut out) and repair by UPR-mortar on the behaviour of slabs. The second group consists of R1, R2, R3 to identify the influence of patched area location on the global response of the slabs. Similar to the first group, the centric concentrated load is also applied. The last group (Figure 7 (c)) are slabs (R1, R4, R5, R6) having similar patched area and location, but the concentrated load is imposed at varying positions. Different to those of the first and second group where the maximum deflections are observed at the centre of the slabs, the maximum deflections of slabs in the third group occur eccentrically following the position of the imposed loads.

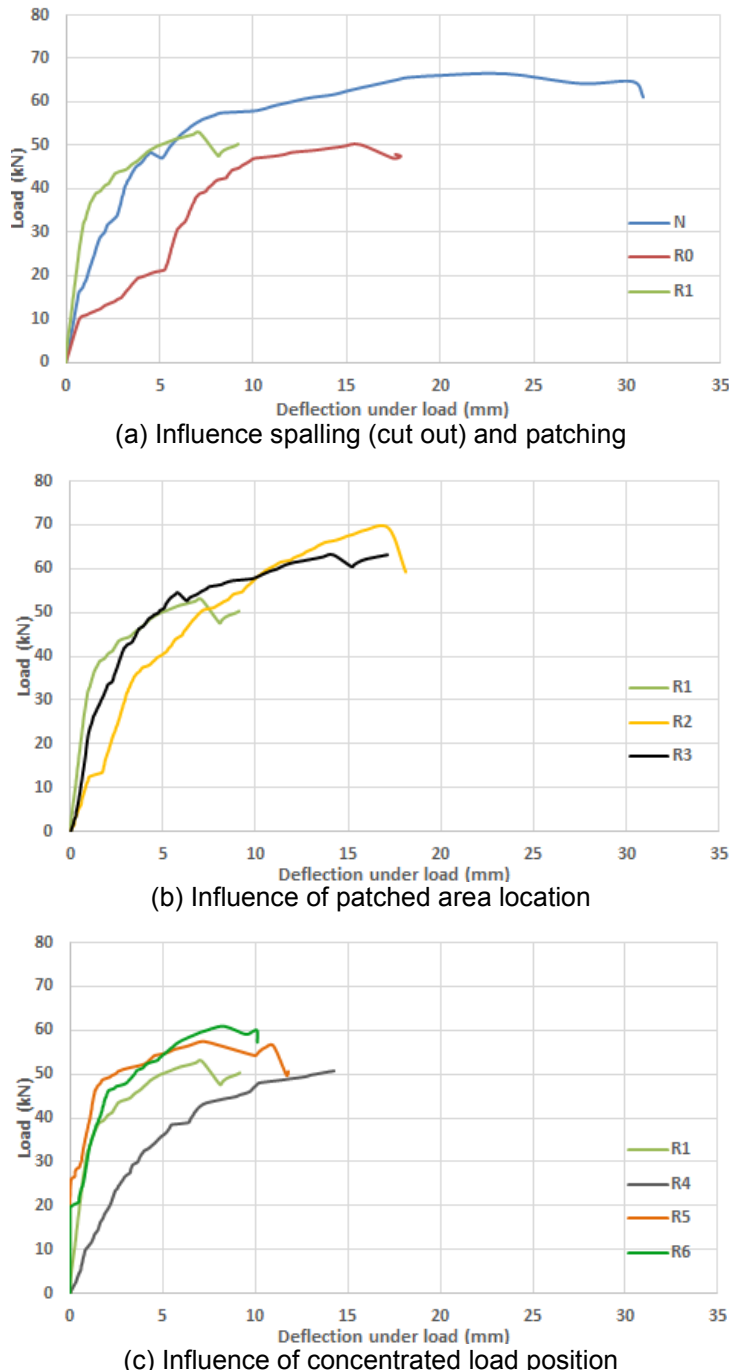


Figure 7. The load-deflection behaviour of the investigated slabs.

Generally, four phases of response can be identified: the first phase is a linear response with a high stiffness up to the initiation of cracks. The load causing the first crack (P_c) and its corresponding deflection (Δ_c) for each slab has been summarised in Table 5. The second phase indicates that the linear behaviour is

maintained but the stiffness of the slab is lower than that of the first phase. The lower stiffness is attributed to the propagation of cracks intensity as the imposed load increases. This phase is end when the reinforcement starts to yield. Table 5 shows the load (P_y) and its corresponding deflection (Δy) at the first yield of the reinforcement for each slab. After the first yield, the slab still capable to receive a higher load but a plastic response can be observed as indicated by large deformation. The peak load (P_u) marks the end of this phase. The value of peak load (P_u) and its corresponding deflection (Δu) for each slab can be seen in Table 5. After peak load, the slab still capable to show ductile behaviour before rupture, in which the slab deforms even though the imposed load is decreased. The maximum deformation (Δ_{max}) when the slab rupture is shown in Table 5.

Table 5. Load-deformation parameters of the slabs.

Slab ID	P_c (kN)	Δc (mm)	P_y (kN)	Δy (mm)	P_u (kN)	Δu (mm)	Δ_{max} (mm)
N	33.57	2.68	47.35	4.47	66.68	19.80	30.89
R0	9.98	0.71	21.21	3.86	50.35	15.70	17.88
R1	32.66	0.98	36.11	1.16	53.07	7.09	9.15
R2	13.61	0.60	36.29	3.58	69.40	17.20	18.12
R3	21.77	0.93	42.18	2.97	63.05	14.20	17.14
R4	23.59	2.47	35.87	3.64	50.80	14.27	15.55
R5	26.31	2.01	46.97	3.80	57.61	7.32	11.71
R6	17.24	0.61	43.72	2.49	60.78	8.38	10.14

There are other important parameters which can be deduced from the load-deflection behaviour i.e. stiffness, toughness, etc [15, 45, 46]. Stiffness indicates the deformation (deflection) resistance of the slab against the imposed load. The value may be determined by the slope of the load-deflection curve from the first initiation of cracks to the deflection equal to 3 mm. However, some of the investigated slabs show the reinforcement is already yielded at a deflection below 3 mm. Hence, for the current research the deflection at the first yield is used instead of the 3 mm limit to determine the stiffness. The characteristic of slab to absorb energy (toughness) can be recognised from the area under load-deflection curve. The value of stiffness and toughness are presented in Table 6.

Table 6. Stiffness and toughness of the slab,

Slab ID	Stiffness (kN/mm)	Toughness (kN.mm)
N	7.70	1774.19
R0	3.57	659.88
R1	19.17	403.59
R2	7.61	897.95
R3	10.00	887.10
R4	10.48	532.90
R5	11.55	607.48
R6	14.09	515.58

The influence of cut out and patching can be observed from Figure 7(a). It is obvious from the figure that spalling of slab (as simulated by cut out) causes reductions of the slab capacity, stiffness and toughness. Application of UPR-mortar to patch the cut out (R1) can be expected to recover the capacity, stiffness and toughness of the slab. However, the increase can only be observed at early phase up to a load of about 50 kN. After this load level, the repaired slab does not show large deformation due to the punching shear and delamination failure mode. It seems that delamination that occur in this slab (see Figure 5 (a)) terminates the response of the slab to receive higher load level. If there is no delamination, UPR-mortar could be effective to restore the deficient capacity and stiffness of spalling slab. This is confirmed by the higher capacity and stiffness of all other repaired slabs compared to those of the slab with cut out (R0). In term of toughness, it seems that UPR-mortar could not restore the toughness to the original toughness of normal slab (N).

The influence of patched area location can be observed from Figure 7 (b). The general trends of the load-deflection curves show similarity. However, there is evident that patched area location affects the characteristic values of strength, stiffness, and toughness of the slab (Table 6). Meanwhile, the influence of concentrated load position can be observed from Figure 7 (c). Except for R4, all other slabs show similar trend of the load-deflection curve. The different in the load-deflection curve of R4 from the other slabs could be associated with the fact that the concentrated load are applied right above the interface between the repair material and substrate concrete (Table 3). This load position will induce stress concentration at the interface leading to high deformation at this location. Hence, the stiffness, toughness and capacity of R4 are lower than others.

4. Conclusions

In this research, experimental investigations have been carried out to determine the cracks pattern and ultimate load of two-way reinforced concrete slabs patched with UPR-mortar under concentrated load, with variations of patching area and load positions. The main conclusions can be stated as follows:

- The development of cracks patterns in both normal slab and patched repair slabs show similarity where the crack is initiated at the tensile side of the slabs at a point under load position. It is interesting to note that the crack lines do not cross the patched area as a result of high flexural strength of the UPR-mortar (24.6 MPa).
- Final crack patterns (failure phase) in normal slab or patched repair slabs tend to form circular-fan pattern. The intensity of the crack lines in the two types of slabs show similarity. This indicates that the use of UPR-mortar as a patch repair material could redistribute the bending moment in similar way to that of normal slab.
- Not all slab specimens have a flexural failure mode, but some specimens show a punching shear mode (R0, R1, R5). Additional delamination of the repair material could occur if the patching process was not done properly (R1).
- The corner levers phenomenon (uplift in the slab corner region) due to the absence of restraint against upward displacement in the slab support affects the yield line patterns in which the yield lines tend to divert toward the side of the slab.
- The simplified YLT has been applied with the principle of virtual work to estimate the ultimate load of the slabs. The results of calculation by simplified YLT theory show that the ultimate strength is at least 90 % compared to the experimental result, except for slab R2.
- The load-deflection behavior of the slabs (either normal or repair) can be identified into four phases: linear response with high stiffness up to first cracks, linear response from the first cracks up to the first yield of reinforcement, plastic response from the first yield to the peak load, and further ductile response from the peak load to the rupture.
- UPR-mortar can recover the capacity and stiffness of the damage (cut out) slab but it cannot restore the toughness to the original value (normal slab).

5. Acknowledgement

The research was financially supported by Universitas Sebelas Maret, Indonesia through Fundamental Research Scheme (Contract No. 543/UN27.21/PP/2018).

References

1. ACI Committee 318. Building Code Requirements for Structural Concrete (ACI 318-14). 22(88)2014.
2. Rombach, G., Kohl, M. Shear design of RC bridge deck slabs according to eurocode 2. *Journal of Bridge Engineering*. 2013. 18(12). Pp. 1261–1269. DOI: 10.1061/(ASCE)BE.1943-5592.0000460.
3. Daniel N. Farhey, Moshe A. Adin, and D.Z.Y. REPAIRED RC FLAT-SLAB-COLUMN SUBASSEMBLAGES UNDER LATERAL LOADING. *Journal of Structural Engineering*. 1995. 121(11). Pp. 1710–1720.
4. Rybakov, V.A., Ananeva, I.A., Rodicheva, A.O., Ogidan, O.T. Stress-strain state of composite reinforced concrete slab elements under fire activity. *Magazine of Civil Engineering*. 2017. 74(6). Pp. 161–174. DOI: 10.18720/MCE.74.13.
5. Eyre, J.R., Nokhasteh, M.A. STRENGTH ASSESSMENT OF CORROSION DAMAGED REINFORCED CONCRETE SLABS AND BEAMS. *Proceedings of the Institution of Civil Engineers – Structures and Buildings*. 1992. 94(2). Pp. 197–203. DOI: 10.1680/istbu.1992.18788.
6. Lushnikova, V.Y., Tamrazyan, A.G. The effect of reinforcement corrosion on the adhesion between reinforcement and concrete. *Magazine of Civil Engineering*. 2018. 80(4). Pp. 128–137. DOI: 10.18720/MCE.80.12.
7. Kim, M.O., Bordelon, A., Lee, M.K., Oh, B.H. Cracking and failure of patch repairs in RC members subjected to bar corrosion. *Construction and Building Materials*. 2016. 107. Pp. 255–263. DOI: 10.1016/j.conbuildmat.2016.01.017.
8. Al-Harthy, A.S., Stewart, M.G., Mullard, J. Concrete cover cracking caused by steel reinforcement corrosion. *Magazine of Concrete Research*. 2011. 63(9). Pp. 655–667. DOI: 10.1680/macr.2011.63.9.655.
9. Mullard, J.A., Stewart, M.G. Corrosion-induced cover cracking: New test data and predictive models. *ACI Structural Journal*. 2011. 108(1). Pp. 71–79. DOI: 10.14359/51664204.
10. Chernin, L., Val, D. V. Prediction of corrosion-induced cover cracking in reinforced concrete structures. *Construction and Building Materials*. 2011. 25(4). Pp. 1854–1869. DOI: 10.1016/j.conbuildmat.2010.11.074.
11. Li, C.Q., Zheng, J.J., Lawanwisut, W., Melchers, R.E. Concrete Delamination Caused by Steel Reinforcement Corrosion. *Journal of Materials in Civil Engineering*. 2007. 19(7). Pp. 591–600. DOI: 10.1061/(ASCE)0899-1561(2007)19:7(591).
12. Chen, Y., Yu, J., Leung, C.K.Y. Use of high strength Strain-Hardening Cementitious Composites for flexural repair of concrete structures with significant steel corrosion. *Construction and Building Materials*. 2018. 167. Pp. 325–337. DOI: 10.1016/j.conbuildmat.2018.02.009.
13. Kim, H., Han, D., Kim, K., Romero, P. Performance assessment of repair material for deteriorated concrete slabs using chemically bonded cement. *Construction and Building Materials*. 2020. 237. Pp. 117468. DOI: 10.1016/j.conbuildmat.2019.117468.
14. Assaad, J.J. Development and use of polymer-modified cement for adhesive and repair applications. *Construction and Building Materials*. 2018. 163. Pp. 139–148. DOI: 10.1016/j.conbuildmat.2017.12.103.

15. Al-Rousan, R., Issa, M., Shabila, H. Performance of reinforced concrete slabs strengthened with different types and configurations of CFRP. *Composites Part B: Engineering*. 2012. 43(2). Pp. 510–521. DOI: 10.1016/j.compositesb.2011.08.050.
16. Pelà, L., Aprile, A., Benedetti, A. Experimental study of retrofit solutions for damaged concrete bridge slabs. *Composites Part B: Engineering*. 2012. 43(5). Pp. 2471–2479. DOI: 10.1016/j.compositesb.2011.08.038.
17. Yin, H., Teo, W., Shirai, K. Experimental investigation on the behaviour of reinforced concrete slabs strengthened with ultra-high performance concrete. *Construction and Building Materials*. 2017. 155. Pp. 463–474. DOI: 10.1016/j.conbuildmat.2017.08.077.
18. Schladitz, F., Frenzel, M., Ehlig, D., Curbach, M. Bending load capacity of reinforced concrete slabs strengthened with textile reinforced concrete. *Engineering Structures*. 2012. 40. Pp. 317–326. DOI: 10.1016/j.engstruct.2012.02.029.
19. Loreto, G., Leardini, L., Arboleda, D., Nanni, A. Performance of RC slab-type elements strengthened with fabric-reinforced cementitious-matrix composites. *Journal of Composites for Construction*. 2014. 18(3). DOI: 10.1061/(ASCE)CC.1943-5614.0000415.
20. Fernandes, H., Lúcio, V., Ramos, A. Strengthening of RC slabs with reinforced concrete overlay on the tensile face. *Engineering Structures*. 2017. 132. Pp. 540–550. DOI: 10.1016/j.engstruct.2016.10.011.
21. Zhu, Y., Zhang, Y., Hussein, H.H., Chen, G. Flexural strengthening of reinforced concrete beams or slabs using ultra-high performance concrete (UHPC): A state of the art review. *Engineering Structures*. 2020. 205(November 2019). Pp. 110035. DOI: 10.1016/j.engstruct.2019.110035.
22. Bonaldo, E., de Barros, J.A., Lourenço, P.B. Efficient Strengthening Technique to Increase the Flexural Resistance of Existing RC Slabs. *Journal of Composites for Construction*. 2008. 12(2). Pp. 149–159. DOI: 10.1061/(ASCE)1090-0268(2008)12:2(149).
23. Radik, M.J., Erdogmus, E., Schafer, T. Strengthening Two-Way Reinforced Concrete Floor Slabs Using Polypropylene Fiber Reinforcement. *Journal of Materials in Civil Engineering*. 2011. 23(5). Pp. 562–571. DOI: 10.1061/(ASCE)MT.1943-5533.0000206.
24. Koutas, L.N., Bournas, D.A. Flexural Strengthening of Two-Way RC Slabs with Textile-Reinforced Mortar: Experimental Investigation and Design Equations. *Journal of Composites for Construction*. 2017. 21(1). Pp. 04016065. DOI: 10.1061/(ASCE)CC.1943-5614.0000713.
25. Chen, D.H., Won, M. Field performance with state-of-the-art patching repair material. *Construction and Building Materials*. 2015. 93. Pp. 393–403. DOI: 10.1016/j.conbuildmat.2015.06.002.
26. Ali, M.S., Leyne, E., Saifuzzaman, M., Mirza, M.S. An experimental study of electrochemical incompatibility between repaired patch concrete and existing old concrete. *Construction and Building Materials*. 2018. 174. Pp. 159–172. DOI: 10.1016/j.conbuildmat.2018.04.059.
27. Abo Sabah, S.H., Hassan, M.H., Muhamad Bunnori, N., Megat Johari, M.A. Bond strength of the interface between normal concrete substrate and GUSMRC repair material overlay. *Construction and Building Materials*. 2019. 216. Pp. 261–271. DOI: 10.1016/j.conbuildmat.2019.04.270.
28. Kristiawan, S.A. Evaluation of Models for Estimating Shrinkage Stress in Patch Repair System. *International Journal of Concrete Structures and Materials*. 2012. 6(4). DOI: 10.1007/s40069-012-0023-y.
29. Yazdi, M.A., Dejager, E., Debraekeleer, M., Gruyaert, E., Van Tittelboom, K., De Belie, N. Bond strength between concrete and repair mortar and its relation with concrete removal techniques and substrate composition. *Construction and Building Materials*. 2020. 230. Pp. 116900. DOI: 10.1016/j.conbuildmat.2019.116900.
30. Nunes, V.A., Borges, P.H.R., Zanotti, C. Mechanical compatibility and adhesion between alkali-activated repair mortars and Portland cement concrete substrate. *Construction and Building Materials*. 2019. 215. Pp. 569–581. DOI: 10.1016/j.conbuildmat.2019.04.189.
31. Stefanus, K., Agus, S., Ageng, B.P., Siti, R. Mechanical properties of unsaturated polyester resin (UPR) – Mortar and its potential application to restore the strength and serviceability Of patched reinforced concrete slab. *Key Engineering Materials*. 2017. 737 KEM. Pp. 560–566. DOI: 10.4028/www.scientific.net/KEM.737.560.
32. Kristiawan, S.A., Fitrianto, R.S. Comparison of shrinkage related properties of various patch repair materials. *IOP Conference Series: Materials Science and Engineering*. 2017. 176. Pp. 012017. DOI: 10.1088/1757-899X/176/1/012017.
33. Adi Kristiawan, S., Bekti Prakoso, A. Flexural Behaviour of Patch-Repair Material Made from Unsaturated Polyester Resin (UPR)-Mortar. *Materials Science Forum*. 2016. 857. Pp. 426–430. DOI: 10.4028/www.scientific.net/MSF.857.426.
34. Kristiawan, S., Supriyadi, A., Pradana, D.R., Azhim, M.R.N. Flexural behaviour of one-way patched reinforced concrete (RC) slab under concentrated load. *Asian Journal of Civil Engineering*. 2018. 19(2). DOI: 10.1007/s42107-018-0014-7.
35. Zheng, Y., Zhou, L., Xia, L., Luo, Y., Taylor, S.E. Investigation of the behaviour of SCC bridge deck slabs reinforced with BFRP bars under concentrated loads. *Engineering Structures*. 2018. 171(April). Pp. 500–515. DOI: 10.1016/j.engstruct.2018.05.105.
36. Zheng, Y., Yu, G., Pan, Y. Investigation of ultimate strengths of concrete bridge deck slabs reinforced with GFRP bars. *Construction and Building Materials*. 2012. 28(1). Pp. 482–492. DOI: 10.1016/j.conbuildmat.2011.09.002.
37. Fang, H., Xu, X., Liu, W., Qi, Y., Bai, Y., Zhang, B., Hui, D. Flexural behavior of composite concrete slabs reinforced by FRP grid facesheets. *Composites Part B: Engineering*. 2016. 92. Pp. 46–62. DOI: 10.1016/j.compositesb.2016.02.029.
38. Alasam, M.A.A. Yield Line Method Applied to Slabs with Different Supports. (December). University of Khartoum, 2006.
39. Quintas, V. Two main methods for yield line analysis of slabs. *Journal of Engineering Mechanics*. 2003. 129(2). Pp. 223–231. DOI: 10.1061/(ASCE)0733-9399(2003)129:2(223).
40. Burgess, I. Yield-line plasticity and tensile membrane action in lightly-reinforced rectangular concrete slabs. *Engineering Structures*. 2017. 138. Pp. 195–214. DOI: 10.1016/j.engstruct.2017.01.072.
41. Bauer, D., Redwood, R.G. Numerical yield line analysis. *Computers and Structures*. 1987. 26(4). Pp. 587–596. DOI: 10.1016/0045-7949(87)90007-1.
42. Salehian, H., Barros, J.A.O. Prediction of the load carrying capacity of elevated steel fibre reinforced concrete slabs [Online]. *Composite Structures*. 2017. 170. Pp. 169–191. DOI: 10.1016/j.compstruct.2017.03.002. URL: <http://dx.doi.org/10.1016/j.compstruct.2017.03.002>.
43. Park, R.; Gamble, W.L. *Reinforced Concrete Slabs*. Second Edi . John Wiley & Sons, Inc. New York, 2000.
44. Buka-Vaivade, K., Sliseris, J., Serdjukas, D., Pakrastins, L., Vatin, N.I. Rational use of HPSFRC in multi-storey building. *Magazine of Civil Engineering*. 2018. 84(8). Pp. 3–14. DOI: 10.18720/MCE.84.1.
45. Al-Rousan, R. Behavior of two-way slabs subjected to drop-weight. *Magazine of Civil Engineering*. 2019. 90(6). Pp. 62–71. DOI: 10.18720/MCE.90.6.
46. Ehsani, R., Sharbatdar, M.K., Kheyroddin, A. Ductility and moment redistribution capacity of two-span RC beams. *Magazine of Civil Engineering*. 2019. 90(6). Pp. 104–118. DOI: 10.18720/MCE.90.10.

Contacts:

Stefanus Kristiawan, s.a.kristiawan@ft.uns.ac.id

Agus Supriyadi, agussupriyadi@staff.uns.ac.id